Quaternary Science Reviews 186 (2018) 17–26

Contents lists available at ScienceDirect

Quaternary Science Reviews

journal homepage: www.elsevier.com/locate/quascirev

A new record of late Pliocene-early Pleistocene aeolian loess–red clay deposits from the western Chinese Loess Plateau and its palaeoenvironmental implications

Jinbo Zan [a], Xiaomin Fang [a, b, *], Weilin Zhang [a], Maodu Yan [a], Dawen Zhang [a]

[a] CAS Center for Excellence in Tibetan Plateau Earth Sciences, Key Laboratory of Continental Collision and Plateau Uplift, Institute of Tibetan Plateau Research, Chinese Academy of Sciences, Beijing, 100101, China
[b] University of Chinese Academy of Sciences, Beijing, 100049, China

ARTICLE INFO

Article history:
Received 5 April 2017
Received in revised form
1 February 2018
Accepted 10 February 2018
Available online 26 February 2018

Keywords:
Plio-Pleistocene transition
Chinese Loess Plateau
Loess-red clay
Paleoclimatology

ABSTRACT

The loess–red clay sequences in northern China provide high-resolution terrestrial records of Asian monsoon evolution and aridification of the Asian interior. To date, however, aeolian deposits of late Pliocene-early Pleistocene age (3.5–2.4 Ma) have only rarely been reported from the western Chinese Loess Plateau (CLP), which significantly hinders our understanding of the distribution of aeolian deposits and the palaeoenvironmental evolution of the region. Here, we present magnetostratigraphic, lithologic and magnetic susceptibility results for two recently-drilled boreholes from the north bank of Baxie River, central Linxia Basin, which are highly correlative with those of the loess–red clay deposits spanning the interval from 3.6 to 2.4 Ma in the eastern CLP. Our results provide the first direct evidence for the occurrence of late Pliocene-early Pleistocene aeolian deposits in the western CLP and provide new insights into the distribution of aeolian deposits in northern China. The spatial coherence of the magnetic susceptibility fluctuations further indicates that magnetic susceptibility is a powerful tool for stratigraphic correlation of late Pliocene aeolian deposits in the western CLP. In addition, our results demonstrate that erosional events may have occurred in the early or middle Pleistocene, and they may provide new insights into the reasons for the absence of loess–red clay deposits from 3.5 to 2.4 Ma in most parts of the western CLP.

1. Introduction

Continuous late Cenozoic loess–red clay sequences are widely distributed in northern China and these aeolian deposits are important terrestrial archives of both palaeomagnetic and palaeoclimatic information (Liu, 1985; Liu et al., 2015; Maher, 2016). They prove the longest and most detailed terrestrial records of changes in the Asian monsoon and of the aridification of the Asian interior (Liu, 1985; Sun et al., 1998a, b; Ding et al., 1998, 2001; An et al., 2001; Guo et al., 2002; Hao and Guo, 2004; Sun et al., 2006; Qiang et al., 2011; Han et al., 2011; Nie et al., 2014; Wang et al., 2015; Zhang et al., 2016; Song et al., 2017a, b). However, there is increasing evidence indicating that the age range and palaeoclimatic significance of the aeolian loess–red clay sequences to the west of the Liupan Mountains differ significantly from those in the eastern Chinese Loess Plateau (CLP) (Burbank and Li, 1985; Rolph et al., 1989; Hao and Guo, 2004; Zhang et al., 2016). In the eastern CLP, it has been suggested that aeolian red clay–loess deposits formed mainly since ~8-7 Ma (Sun et al., 1998a,b; Ding et al., 1998, 2001; An et al., 2001; Nie et al., 2014; Song et al., 2017a). Magnetic susceptibility and grain size can be used as indicators of the intensity of the East Asian summer and winter monsoons respectively (An et al., 2001; Sun et al., 2006; Nie et al., 2014). However, aeolian deposits of late Pliocene-early Pleistocene age (3.5–2.4 Ma) have only rarely been reported from the western CLP, although typical aeolian deposits have been dated to as early as 22–25 Ma (Guo et al., 2002; Qiang et al., 2011). Magnetic susceptibility measurements have proven useful for stratigraphic correlation in the eastern CLP; however, the magnetic susceptibility

* Corresponding author. CAS Center for Excellence in Tibetan Plateau Earth Sciences, Key Laboratory of Continental Collision and Plateau Uplift, Institute of Tibetan Plateau Research, Chinese Academy of Sciences, Beijing, 100101, China.
E-mail addresses: zanjb@itpcas.ac.cn (J. Zan), fangxm@itpcas.ac.cn (X. Fang), zhangwl@itpcas.ac.cn (W. Zhang), maoduyan@itpcas.ac.cn (M. Yan), zhangdawen@itpcas.ac.cn (D. Zhang).

https://doi.org/10.1016/j.quascirev.2018.02.010
0277-3791/

variations within coeval red clay sequences in the western CLP and the eastern CLP, which are divided by the Liupan Mountains (Fig. 1a), have not been correlated successfully during the interval from ~8 to 3.5 Ma (Hao and Guo, 2004). These observations raise the following questions: Are there continuous late Pliocene-early Pleistocene aeolian red clay-loess sequences in the western CLP? Why are they absent from most parts of the western CLP? Can the magnetic susceptibility record of the late Pliocene red clay from the western CLP be used for stratigraphic correlation, and is the record coherent with that of the eastern CLP? To address these questions, new late Pliocene aeolian sequences in the western CLP need to be investigated.

Thick red beds and subsequent aeolian deposits have accumulated in Linxia Basin since the late Cenozoic (Fig. 1a). Early studies demonstrated that the early Pleistocene *Equus* fauna (2.5–2.2 Ma), excavated from the Longdan section on the south bank of Baxie River (Fig. 1a), was very likely to have been derived from loess deposits (Qiu et al., 2004). However, recent lithological and magnetic susceptibility analyses have demonstrated that aeolian materials from the Longdan section have been subjected to significant post-depositional reworking by water (Zan et al., 2016). Nevertheless, it is possible that further investigations of the red beds overlying the uppermost conglomerate layer along Baxie River (Fig. 1b) could provide new insights into the aeolian deposits of late Pliocene-early Pleistocene age in the western CLP.

Here, we present magnetostratigraphic, lithologic and magnetic susceptibility results for two newly-drilled boreholes from the highest platform surface on the north bank of Baxie River. Our results suggest an aeolian origin of these late Pliocene sequences and provide an opportunity to address the research questions mentioned above.

2. General setting

In 2015 two borehole cores, ~10 km apart, were successfully retrieved from Guonigou (GNG, 35°33′ N, 103°25′E) and Nalesi (NLS, 35°33′ N, 103°30′E) on the north bank of Baxie River (Fig. 1). The NLS and GNG boreholes were drilled to depths of 161 m and 99 m, respectively, and both penetrated the red beds and reached the upper part of the conglomerate layer (Fig. 1b). Based on colour and texture, the lithostratigraphy of both the GNG and NLS boreholes can be divided into five stratigraphic units (Fig. 2):

Unit I (156–161 m in NLS and 95–99 m in GNG) - thick conglomerate layer. The gravel clasts have subrounded to subangular shapes and are strongly carbonate-cemented; the lithology is mainly limestone and quartzite, but metasandstone and granite clasts are also present. Along Baxie River, the conglomerate layer is relatively thick (8–15 m) and widely and uniformly distributed.

Unit II (90–156 m in NLS and 45–95 m in GNG) - Red Clay. The sediments in this unit are reddish brown (5 YR - dry Munsell colour), uniform in composition, and have a moderate to strong subangular blocky structure with occasional clay and iron/manganese coatings. As in the case of the late Pliocene *Hipparion* Red Earth deposits from the eastern CLP, the loess and palaeosol layers could not be clearly distinguished. Small pebbles and numerous well-distributed calcareous concretions are present in the lowermost part of the unit.

Unit III (58–90 m in NLS and 23–45 m in GNG) - alternating reddish soils and yellow-brown loess horizons. The unit consists of clear alternations of five visually-distinct soil and loess layers ("S" and "L" designate palaeosol and loess layers, respectively). Loess layers are yellow-brown to reddish in colour (10 YR to 7.5 YR) and are well cemented and densely jointed. The intervening palaeosols are reddish (5 YR 5/6), characterized by strong clay illuviation and abundant iron/manganese coatings. These characteristics resemble those of the Wucheng loess-palaeosol sequences in the eastern CLP (Liu, 1985).

Unit IV (34–58 m in NLS and 18–23 m in GNG) - loess deposits reworked by water). The unit consists of loess deposits intercalated with thick bluish-gray or black-gray silt layers. The bluish-gray or black-gray silt layers contain abundant oxidation spots and are clearly and finely stratified, which was possibly caused by sheet-flow processes due to the undulating palaeotopography. The palaeosols are weakly developed. Lithofacies and sedimentary characteristics indicate that the stratigraphic contact between Units III and IV may be unconformable.

Unit V (0–34 m in NLS and 0–18 m in GNG) - Malan/Lishi loess deposits. This unit is gray or light grayish yellow in colour (10 YR 5/4), massive, with a uniform composition and loose texture. Many biochannels and carbonate coatings are present in the upper part. The paleosols are well developed in the intervals of 13–16 m in the GNG section and 21–27 m in the NLS section.

3. Materials and methods

A total of 560 and 270 block samples were taken at 25–40-cm intervals from the NLS and GNG borehole cores, respectively. The block samples were cut into 2-cm cubes and demagnetized in a MMTD80 thermal demagnetizer. Most of the samples were subjected to progressive thermal demagnetization in 20 steps, varying between 10 and 50 °C. To minimize possible phase transformations of magnetic minerals, samples from the black-gray or bluish-gray silt layers were subjected to stepwise alternating-field (AF) demagnetization at fields up to 140 mT at 5 or 10 mT increments. All measurements of the natural remanent magnetization were made using a 2G Enterprises Model 755 cryogenic magnetometer installed in a field-free space (<150 nT) at the Institute of Tibetan Plateau Research, Chinese Academy of Sciences.

Low-field magnetic susceptibility was measured at frequencies of 470 and 4700 Hz using a Bartington Instruments meter and MS2B sensor. Frequency dependent susceptibility (χ_{fd}) was calculated as $\chi_{fd} = \chi_{470Hz} - \chi_{4700Hz}$. Low-field temperature-dependent magnetic susceptibility (κ-T) was measured on selected samples using a MFK1-FA Kappabridge equipped with a CS-4 high-temperature furnace (Agico Ltd., Brno, Czech Republic). The κ-T curves were measured from room temperature to 700 °C in an argon atmosphere to minimize oxidation. Grain-size analyses were conducted using a Mastersizer 3000 laser Particle Size Analyzer at the Institute of Tibetan Plateau Research, Chinese Academy of Sciences. Prior to grain-size measurements, organic matter and carbonates were removed using conventional pre-treatment procedures (Konert and Vandenberghe, 1997).

4. Results

The κ-T curves for the samples from the Nalesi (NLS) and Guonigou (GNG) boreholes all exhibit a rapid loss of susceptibility at about 585 °C (Fig. 3), indicating the presence of magnetite. For most of the selected samples, a dramatic loss of susceptibility occurs between 300 and 450 °C, which can be ascribed to the conversion of ferrimagnetic maghemite to weakly magnetic hematite. The loss of susceptibility between 300 and 450 °C in the κ-T curves is more significant in the palaeosol layers than that in the loess layers, suggesting that the soil samples were subjected to stronger pedogenesis and are enriched in fine-grained maghemite particles (Deng et al., 2000; Zan et al., 2017). A further minor fall in magnetic susceptibility between 585 °C and 680 °C (Fig. 3), evident in all the samples, indicates the presence of hematite. Most samples exhibit a clear 'hump' at ca. 520 °C in their heating curves, which can be ascribed either to the Hopkinson effect (Dunlop and Özdemir, 1997)

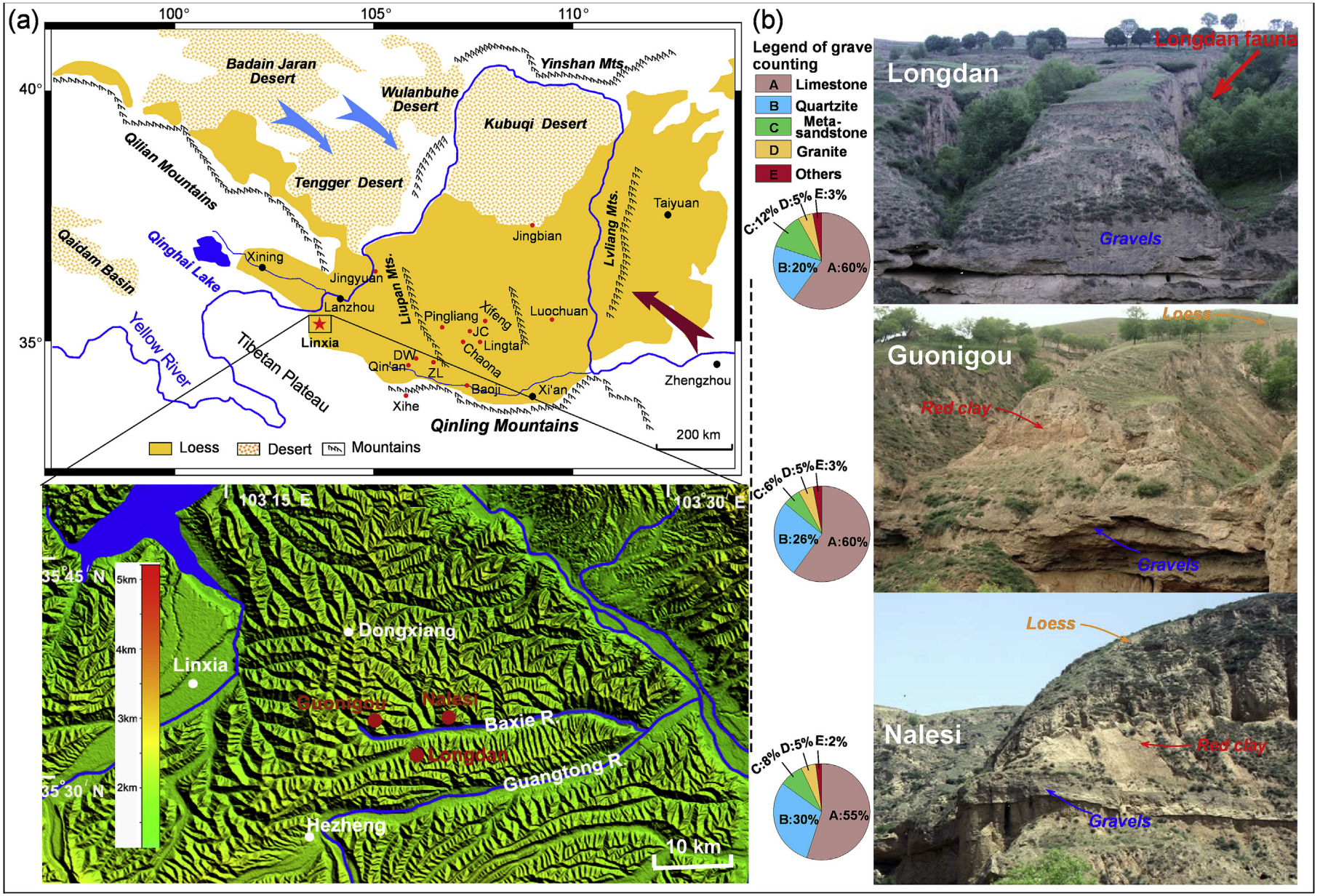

Fig. 1. (a) Top: Locations of Linxia Basin and representative loess-red clay sections in the Chinese Loess Plateau. Blue and red arrows indicate the trajectories of the East Asian winter and summer monsoons, respectively. Bottom: DEM map of Linxia Basin (data from http://www.cgiar-csi.org/data) showing locations of the Guonigou and Nalesi borehole sites. DW: Dongwan; ZL: Zhuanglang borehole; JC: Jingchuan. (b) The uppermost conglomerate layers in the Longdan, Nalesi and Guonigou sections along Baxie River. Reference to the pie chart to the left of each photograph indicates that the conglomerate layers from the three sections have a similar lithology and gravel composition and thus can be used as a regional stratigraphic marker. The early Pleistocene *Equus* fauna found in the Longdan section has an age range of about 2.5–2.2 Ma. (For interpretation of the references to colour in this figure legend, the reader is referred to the Web version of this article.)

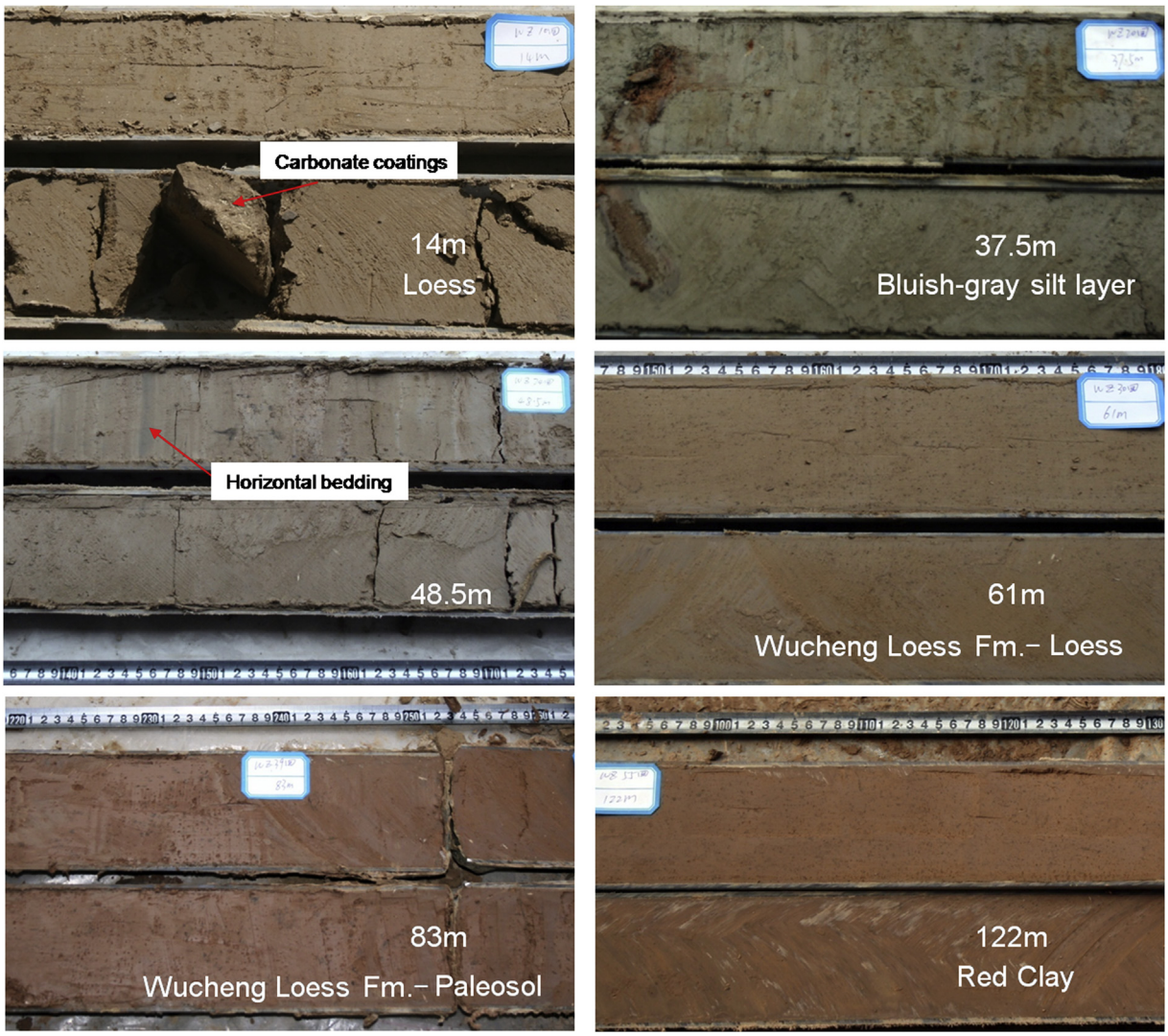

Fig. 2. Photographs illustrating lithological variations in the Nalesi borehole core. Note the oxidation spots and well-defined fine stratification in the bluish-gray silty sediments and the alternating soil and loess layers in the Wucheng Loess Formation.

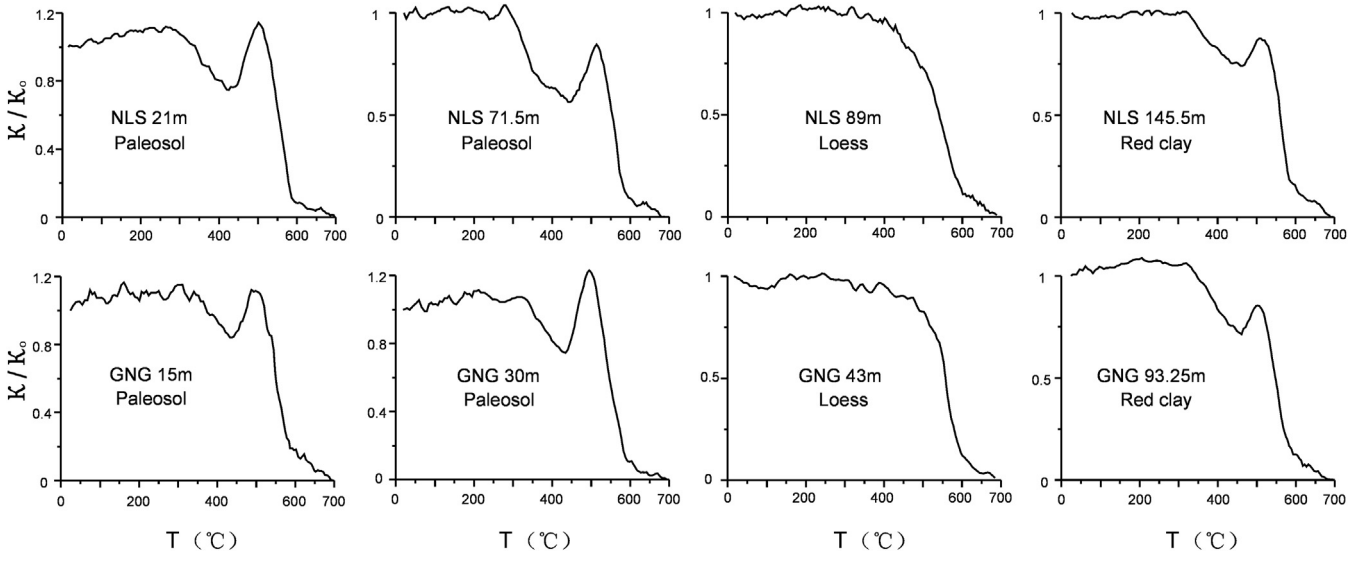

Fig. 3. Variation of magnetic susceptibility with temperature (κ-T curves) of typical samples from the Nalesi (NLS) and Guonigou (GNG) borehole cores.

or to the production of magnetite or other higher susceptibility phases during heating. These types of behavior indicate that magnetite, maghemite and hematite are contributors to the magnetic susceptibility, with magnetite and maghemite making major contributions.

Thermal demagnetization analyses revealed that the characteristic remanent magnetization (ChRM) component was successfully isolated between 250 °C and 670 °C, and decayed almost linearly to the origin after the removal of a secondary magnetization component below 200–250 °C (Fig. 4). The ChRM was calculated using principal component analysis (Kirschvink, 1980), with at least three consecutive steps trending towards the origin above 300 °C. Samples with random directions or with maximum angular deviations (MAD) > 15° were not used for further magnetostratigraphic analyses. Overall, 501 ChRM directions (90%) from the NLS borehole and 236 ChRM directions (87%) from the GNG borehole yielded reliable results. A minimum of two consecutive samples with the same polarity was regarded as representing a possible polarity zone. Four pairs of normal (N1 to N4) and reversed (R1 to R4) polarity zones were identified in the NLS borehole (Fig. 5); and four normal and three reversed polarity zones, designated N1–N4 and R1–R3, respectively, were observed in the GNG borehole (Fig. 5). No palaeomagnetic data are available for the depths of 71–77 m in the GNG borehole due to the occurrence of small pebbles and calcareous concretions. A reversal test was used to assess the nature of the primary ChRM directions (Arason and Levi, 2010). Both boreholes exhibit a difference of <4°between the mean normal and reversed inclination values,

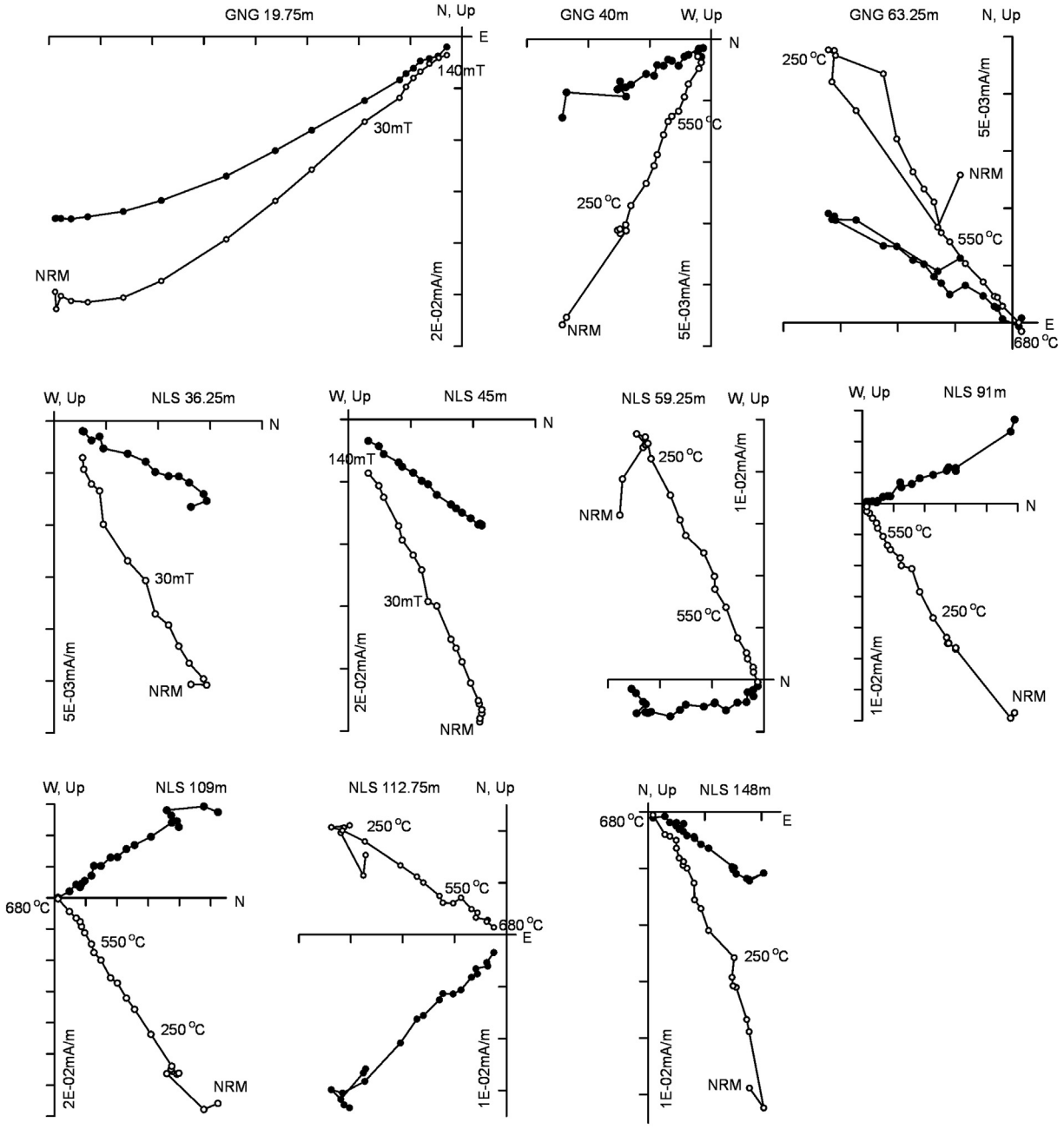

Fig. 4. Results of thermal and alternating-field demagnetization of typical samples from the Nalesi (NLS) and Guonigou (GNG) borehole cores. Solid/open circles represent horizontal/vertical projections.

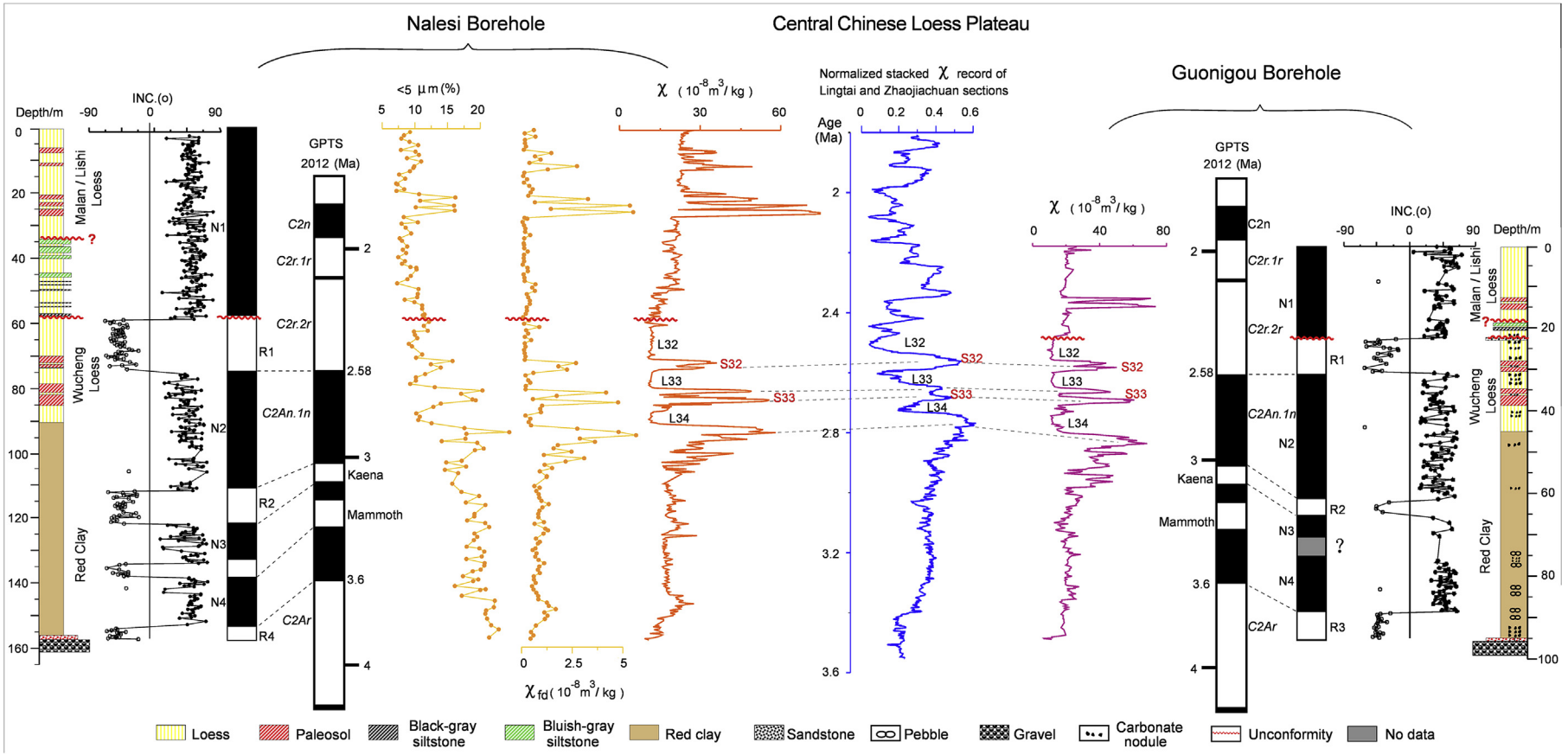

Fig. 5. Magnetostratigraphy, grain size and magnetic susceptibility records of the Nalesi and Guonigou boreholes and correlation with the geomagnetic polarity timescale (GPTS) (Gradstein et al., 2012). Note that the magnetostratigraphic, lithologic and magnetic susceptibility records of the two boreholes are well-correlated with those of the 3.6–2.4 Ma loess–red clay deposits from the Zhaojiachuan and Lingtai sections in the eastern CLP (Sun et al., 2006). The timescale of the composite susceptibility record from the Zhaojiachuan and Lingtai sections was established by astronomical tuning. (For interpretation of the references to colour in this figure legend, the reader is referred to the Web version of this article.)

suggesting an antipodal distribution in the reversed geomagnetic fields (Fig. 6), and thus that the magnetostratigraphic results are reliable.

Field observations and measurements of gravel composition indicate that the uppermost conglomerate layers along Baxie River have a comparable lithology, facies, grain roundness, sorting and cementation (Fig. 1b), and thus they can be regarded as a regional stratigraphic marker. Previous palaeomagnetic work demonstrated that the early Pleistocene *Equus* fauna found in the water-reworked loess deposits above the conglomerate bed (Fig. 1b) had an approximate age of 2.5–2.2 Ma (Zan et al., 2016), and that the uppermost conglomerate layer in the Longdan section had an age range of 4.1- >3 Ma (Zan et al., 2016; Fang et al., 2016). Based on these age constraints, the interval from 74 to 153 m in the NLS borehole is correlated with the Gauss normal chron in the geomagnetic polarity timescale (Gradstein et al., 2012) and thus the two reversed polarity zones correspond to the Kaena and Mammoth subchrons (Fig. 5). Consequently, the reversed polarity zone R1 is correlated with subchron C2r.2r of the Matuyama epoch. In western Linxia Basin, previous studies have demonstrated that the Brunhes/Matuyama boundary was located at the depths of 30–60 m in the Pleistocene loess-palaeosol sequences (Li et al., 1997). The Malan loess deposits from older terraces generally have a thickness of less than 10 m (Li et al., 1997). In addition, a distinctive long Olduvai normal polarity subzone was identified in the water-reworked loess deposits from the Longdan section (Zan et al., 2016) and the fluvial-lacustrine deposits of the Dongshanding section from western Linxia Basin (Fang et al., 2016). According to these observations, the upper part of the thick polarity zone N1 may be correlated with the Brunhes normal polarity zone and the lower water-reworked loess deposits are probably correlated with the Olduvai subchron. This interpretation suggests the presence of a sedimentary hiatus between the Malan-Lishi loess deposits and the water-reworked loess deposits. However, most of the results are preliminary, and more detailed work is needed in the future. Nevertheless, these interpretations imply the presence of an unconformity between polarity zones N1 and R1, which is consistent with the lithological variations.

Extrapolation of the sedimentation rate based on recognition of the Gauss chron yields a basal age of 3.65 Ma for the NLS borehole. The boundary between the upper water-reworked loess and lower loess-soil sequence is at around 2.36 Ma. Except for the absence of the Mammoth subchron, the GNG borehole generally exhibits a similar magnetostratigraphic framework to the NLS borehole and can also be correlated with chrons C2r.2r-C2Ar (Fig. 5) in GPTS 2012. Assuming a sedimentation rate of ~5.8 cm/ky in the Gauss chron, the age of the GNG borehole below the water-reworked loess deposits could be ~2.4 to ~3.7 Ma.

The grain size and magnetic susceptibility records of the NLS borehole sediments both exhibit strong contrasts between palaeosol and loess layers (Fig. 5). The <5 μm grain size fraction and the magnetic susceptibility values are higher in the palaeosols than in the loess. Similar characteristics were also observed in the loess-palaeosol sequences from the eastern CLP (Liu, 1985). Grain-size distributions of representative loess–red clay samples from the NLS borehole and the Chaona section from the eastern CLP are given in Fig. 7a. All are generally composed of a coarse component (ca. 6–60 μm) and a fine overlapping component (ca. < 6 μm), and there is an extended fine tail. These characteristics are typical of aeolian deposits (Liu, 1985).

5. Discussion

To date, aeolian deposits of late Pliocene-early Pleistocene age (3.5–2.4 Ma) have barely been reported from the western CLP. Previous studies demonstrated that the late Pliocene sediments from the Longdan section on the south bank of Baxie River were possibly of aeolian origin (Qiu et al., 2004). Recently, we conducted detailed lithologic and rock magnetic investigations on that section and found that palaeosols were weakly developed throughout the entire section and that the magnetic susceptibility was consistently low (Zan et al., 2016). These characteristics, combined with the

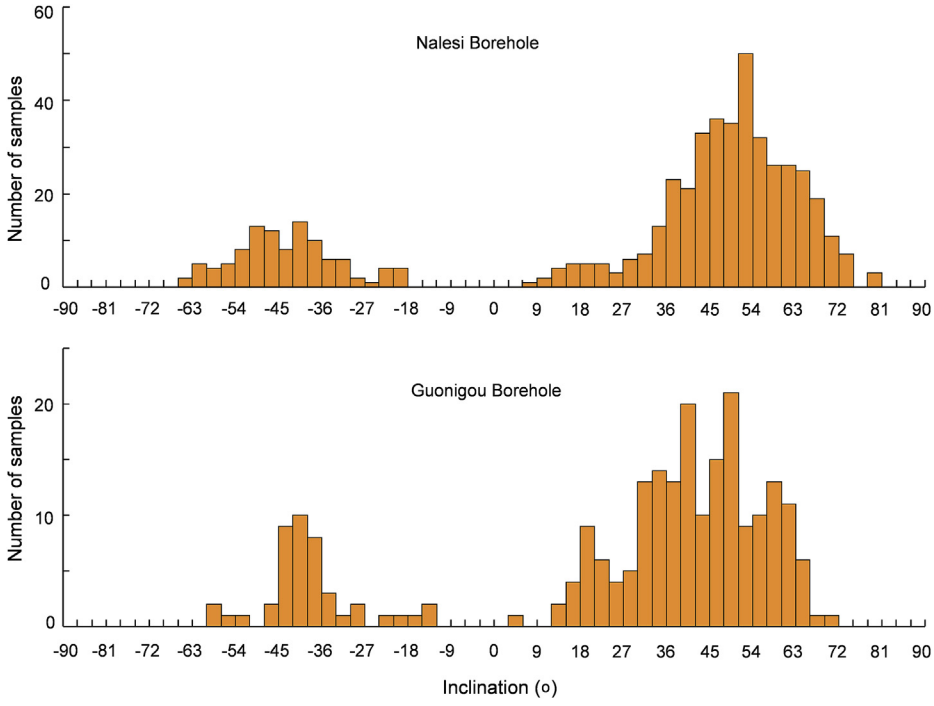

Fig. 6. Histograms of the inclinations of the Nalesi and Guonigou boreholes in 3°bins.

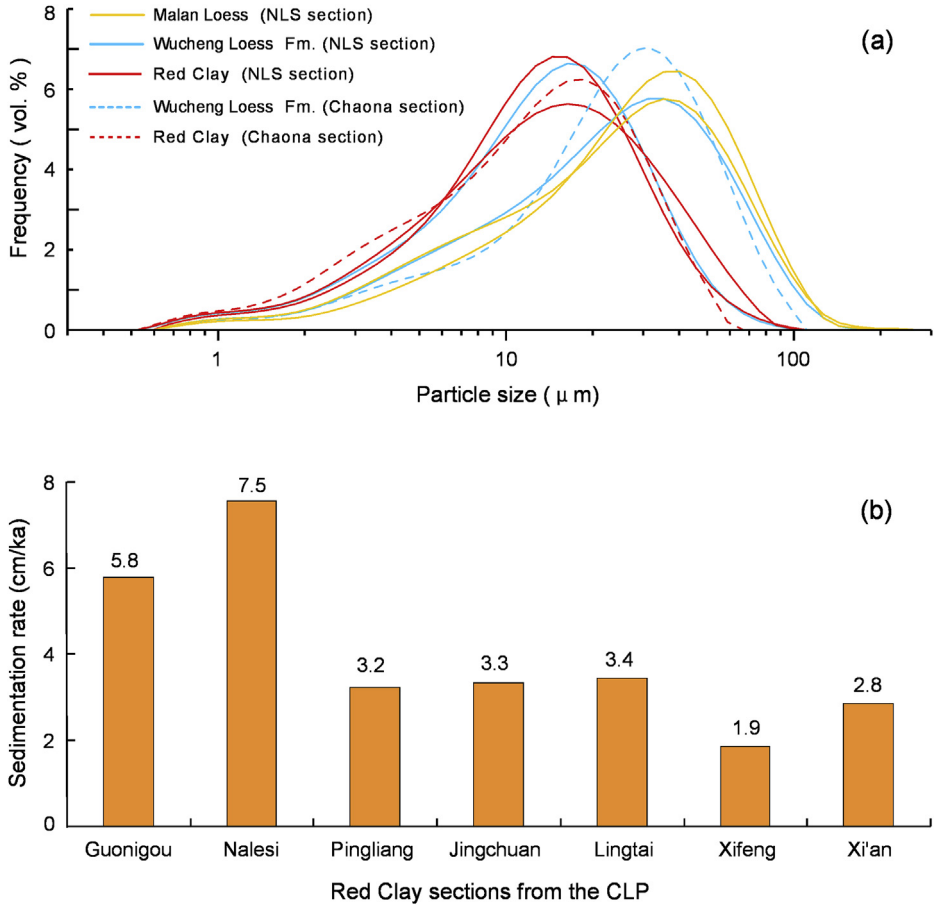

Fig. 7. (a) Comparison of the grain-size distribution of representative loess–red clay samples of the NLS borehole and the Chaona section from the eastern CLP. (b) Sedimentation rates for the interval of the Gauss chron in boreholes GNG and NLS and comparison with the sedimentation rates of contemporaneous red clay sequences from the eastern CLP (Sun et al., 1997, 1998a, b; Ding et al., 1998, 2001). The sites are arranged approximately from west (left) to east (right). (For interpretation of the references to colour in this figure legend, the reader is referred to the Web version of this article.)

occurrence of bluish-gray silt layers and sub-horizontal bedding, suggest that aeolian materials from the Longdan area were reworked by water. These observations also imply that the late Pliocene-early Pleistocene red clay–loess sequences are probably distributed in many areas of the central Linxia Basin. Our lithologic, magnetostratigraphic and rock magnetic analyses of the GNG and NLS boreholes provide further support for this inference.

Magnetic susceptibility has been used for stratigraphic correlation of aeolian loess–red clay sequences in the eastern CLP (Sun et al., 2006; Yang and Ding, 2010). In the eastern CLP, the Matuyama/Gauss boundary is generally located in loess layer L33 (Sun et al., 2006; Yang and Ding, 2010). In addition, loess/palaeosols units S33 and L34 from the eastern CLP, which were recently characterized based on new analyses of their litho- and pedostratigraphic features and magnetic susceptibility (Yang and Ding, 2010), both fall within subchron C2An.1n. All these characteristics are also observed in the GNG and NLS drill cores. These observations provide important constraints on our magnetostratigraphic interpretations and suggest that our magnetostratigraphic age determinations are probably reliable.

In addition, the magnetic susceptibility records of the GNG and NLS boreholes, which are located about 10 km apart, exhibit remarkably similar variations (Fig. 5). Moreover, their long-term changes are both highly correlated with those of the 3.6–2.4 Ma astronomically-tuned loess–red clay sequences from the Zhaojiachuan and Lingtai sections in the eastern CLP, characterized by higher values in palaeosol units S32 and S33, and lower values in loess layers L32, L33 and L34 (Fig. 5). χ_{fd}, which is regarded as a sensitive parameter of the degree of pedogenesis (Maher, 2016), also exhibits higher values in the palaeosol units and lower values in the loess layers (Fig. 5). In addition, our preliminary thermomagnetic analyses of the borehole samples demonstrate that the loss of susceptibility between 300 and 450 °C in the κ-T curves is more significant in the palaeosol layers than in the loess layers (Fig. 3), suggesting that the soil samples were subjected to stronger pedogenesis and are enriched in fine-grained maghemite particles (Deng et al., 2000; Zan et al., 2017). The spatial coherence of susceptibility fluctuations, together with a pedogenic model of magnetic susceptibility enhancement, is also reported for Late Pliocene-Early Pleistocene loess–red clay deposits from the eastern CLP (Sun et al., 2006; Yang and Ding, 2010).

The grain-size distributions of representative loess–red clay samples from the NLS borehole are characteristic of aeolian deposits (Fig. 7a). The median grain-size of the Malan loess deposits ranges from 40 to 60 μm, much coarser than the samples from the Wucheng loess Fm. and the red clay deposits from Linxia Basin. This pattern of temporal variation in grain size is also consistent with that of the aeolian deposits form the eastern CLP (Liu, 1985).

The linear sedimentation rate (LSR) of the interval corresponding to the Gauss chron in boreholes GNG and NLS is ~7.5 cm/ky and ~5.8 cm/ky, respectively, which is roughly twice that of most of the late Pliocene *Hipparion* Red Earth sites in the eastern Loess Plateau

(Fig. 7b). This spatial pattern resembles that of the Quaternary loess deposits in the western CLP where higher sedimentation rates are also observed (Liu, 1985; Zhang et al., 2016). For example, the LSR of the Xijin loess near Lanzhou, which has a basal age of 2.2 Ma (Zhang et al., 2016), is around 18.9 cm/ky and roughly 2–3 times higher than that of the eastern CLP (5.3–6.7 cm/ky).

At present, the origin of Neogene red beds in the western CLP remains controversial. In most previous studies, the presence of yellow-brown siltstone or sandstone with a uniform composition and massive structure is generally considered evidence for an aeolian origin. Based on investigations of sedimentary facies and analysis of multi-proxy indices, our results represent the first identification of aeolian sequences from the western CLP that are of late Pliocene-early Pleistocene age. Our results also demonstrate that magnetic susceptibility can be used as a powerful tool for identifying late Pliocene-early Pleistocene eolian deposits in the western CLP. In addition, the magnetic susceptibility records from the GNG and NLS boreholes are highly correlative with those of the contemporaneous loess–red clay sequences in the eastern CLP, strongly indicating that the magnetic susceptibility proxy record of Linxia Basin can be used to reflect long-term variations in the East Asian summer monsoon.

In summary, these well-preserved aeolian deposits from Linxia Basin extend the upper limit of the previously-reported Miocene loess-palaeosol sequences in Tianshui Basin (Guo et al., 2002; Hao and Guo, 2004) to the early Quaternary, about 2.36 Ma, and provide a rare window into the late Pliocene-Pleistocene distribution of aeolian sediments and palaeoenvironmental evolution on the NE margin of the Tibetan Plateau. Combined with the newly-discovered Xijin loess (2.2 Ma to present) from Lanzhou Basin (Zhang et al., 2016), the loess–red clay sequences from the western CLP potentially constitute a complete sequence of aeolian strata spanning the last 25 Ma in northern China (Guo et al., 2002; Hao and Guo, 2004; Qiang et al., 2011).

Aeolian deposits are extremely sensitive to erosional processes and their preservation requires a relatively stable tectonic/geomorphic environment during and after their deposition. Thus, investigations of the temporal continuity of the GNG and NLS borehole cores may provide additional information about tectonically-induced deformation and associated erosion. In the upper part of the GNG and NLS boreholes, an unconformity between the water-reworked loess deposits and the Wucheng Loess Formation was identified based on lithologic variations and magnetostratigraphic correlations (Fig. 5). In addition, the bluish-gray or black-gray silt layers contain well-defined fine stratifications and abundant oxidation spots, indicating sheet-flow processes that may have been induced by tectonically-induced erosion when the aeolian materials were deposited.

At present, there is considerable evidence for growth of the northern Tibetan Plateau during the early or middle Pleistocene (Pan et al., 2009; Li et al., 2014; Gao et al., 2017), supporting the view that aeolian materials from Linxia Basin were probably affected by tectonically-induced erosional events after 2.4 Ma. A detailed palaeomagnetic study of the fluviolacustrine sedimentary sequence in the western Linxia Basin indicates that the deposition of fluvial-lacustrine sediments was terminated after 1.8 Ma by pulsed tectonic deformation and uplift of the entire Linxia Basin (Fang et al., 2016).

6. Conclusions

Lithologic, low-field magnetic susceptibility, and magnetostratigraphic analyses of the GNG and NLS boreholes demonstrate the occurrence of well-preserved aeolian loess–red clay sequences in the central part of Linxia Basin corresponding to the time interval from 3.6 to 2.4 Ma. These boreholes represent the first evidence of late Pliocene-early Pleistocene aeolian sequences recovered from the western CLP. The major trends of the magnetic susceptibility records from the two boreholes are highly correlative with those of contemporaneous loess–red clay sequences in the eastern CLP, suggesting that this parameter can be used both for stratigraphic and palaeoclimatic correlation and as a powerful tool for identifying late Pliocene-early Pleistocene aeolian deposits in the western CLP. The occurrence of erosional events in both the early or middle Pleistocene, indicated by several stratigraphic unconformities above the Wucheng Loess, may provide new clues into the reasons for the absence of late Pliocene-early Pleistocene aeolian deposits in most parts of the western CLP.

Acknowledgements

This work was co-supported by the National Natural Science Foundation of China (grants 41571198, 41620104002), the National Basic Research Program of China (grant 2017YFC0602803), and the Youth Innovation Promotion Association, CAS, China (grant 2016071). We thank Dr. Jan Bloemendal for suggestions for improving the manuscript.

References

An, Z., Kutzbach, J.E., Prell, W.L., Porter, S.C., 2001. Evolution of Asian monsoons and phased uplift of the Himalayan Tibetan plateau since Late Miocene times. Nature 411, 62–66. https://doi.org/10.1038/35075035.

Arason, P., Levi, S., 2010. Maximum likelihood solution for inclination-only data in paleomagnetism. Geophys. J. Int. 182, 753–771. https://doi.org/10.1111/j.1365-246X.2010.04671.x.

Burbank, D.W., Li, J., 1985. Age and palaeoclimatic significance of the loess of Lanzhou, north China. Nature 316, 429–431. https://doi.org/10.1038/316429a0.

Deng, C.L., Zhu, R.X., Verosub, K.L., Singer, M.J., Yuan, B.Y., 2000. Paleoclimatic significance of the temperature-dependent susceptibility of Holocene loess along a NW-SE transect in the Chinese loess plateau. Geophys. Res. Lett. 27, 3715–3718. https://doi.org/10.1029/2000GL008462.

Ding, Z.L., Sun, J.M., Yang, S.L., Liu, T.S., 1998. Preliminary magnetostratigraphy of a thick eolian red clay-loess sequence at Lingtai, the Chinese Loess Plateau. Geophys. Res. Lett. 25, 1225–1228. https://doi.org/10.1029/98GL00836.

Ding, Z.L., Yang, S.L., Hou, S.S., Wang, X., Chen, Z., Liu, T.S., 2001. Magnetostratigraphy and sedimentology of the Jingchuan red clay section and correlation of the Tertiary eolian red clay sediments of the Chinese Loess Plateau. J. Geophys. Res. 106, 6399–6407. https://doi.org/10.1029/2000JB900445.

Dunlop, D.J., Özdemir, Ö., 1997. Rock Magnetism: Fundamentals and Frontiers. Cambridge Univ. Press, New York, pp. 572–573.

Fang, X.M., Wang, J.Y., Zhang, W.L., Zan, J.B., Song, C.H., Yan, M.D., Appel, E., Zhang, T., Wu, F.L., Yang, Y.B., Lu, Y., 2016. Tectonosedimentary evolution model of an intracontinental flexural (foreland) basin for paleoclimatic research. Global Planet. Change 145, 78–97. https://doi.org/10.1016/j.gloplacha.2016.08.015.

Gao, H.S., Li, Z.M., Liu, X.F., Pan, B.T., Wu, Y.J., Liu, F.L., 2017. Fluvial terraces and their implications for Weihe River valley evolution in the Sanyangchuan Basin. Sci. China Earth Sci. 60, 413–427. https://doi.org/10.1007/s11430-016-5037-8.

Gradstein, F., Ogg, J.G., Schmitz, M., Ogg, G., 2012. The Geologic Time Scale 2012. Elsevier, Oxford, UK, 1144 p.

Guo, Z.T., Ruddiman, W.F., Hao, Q.Z., Wu, H.B., Qiao, Y.S., Zhu, R.X., Peng, S.Z., Wei, J.J., Yuan, B.Y., Liu, T.S., 2002. Onset of Asian desertification by 22 Myr ago inferred from loess deposits in China. Nature 416, 159–163. https://doi.org/10.1038/416159a.

Han, W.X., Fang, X.M., Berger, A., Yin, Q.Z., 2011. An astronomically tuned 8.1 Ma eolian record from the Chinese Loess Plateau and its implication on the evolution of Asian monsoon. J. Geophys. Res. 116 https://doi.org/10.1029/2011JD016237.

Hao, Q.Z., Guo, Z.T., 2004. Magnetostratigraphy of a late Miocene-Pliocene loess-soil sequence in the western Loess Plateau in China. Geophys. Res. Lett. 31, L09209 https://doi.org/10.1029/2003GL019392.

Kirschvink, J.L., 1980. The least-squares line and plane and the analysis of palaeomagnetic data. Geophys. J. Int. 62, 699–718. https://doi.org/10.1111/j.1365-246X.1980.tb02601.x.

Konert, M., Vandenberghe, J., 1997. Comparison of laser grain size analysis with pipette and sieve analysis: a solution for the underestimation of the clay fraction. Sedimentology 44, 523–535.

Li, J.J., Fang, X.M., Van der Voo, R., Zhu, J.J., MacNiocaill, C., Onto, Y., Pan, B.T., Zhong, W., Wang, J.L., Sasaki, T., Zhang, Y.T., Cao, J.X., Kang, S.C., Wang, J.M., 1997. Magnetostratigraphic dating of river terraces: rapid and intermittent incision by the Yellow River of the northeastern margin of the Tibetan Plateau during the Quaternary. J. Geophys. Res. 102, 10121–10132.

Li, J.J., Fang, X.M., Song, C.H., Pan, B.T., Ma, Y.Z., Yan, M.D., 2014. Late Miocene-Quaternary rapid stepwise uplift of the NE Tibetan Plateau and its effects on climatic and environmental changes. Quat. Res. 81, 400–423.

Liu, T.S. (Ed.), 1985. Loess and the Environment. China Ocean press, Beijing, pp. 1–251.

Liu, Q.S., Jin, C.S., Hu, P.X., Jiang, Z.X., Ge, K.P., Roberts, A.P., 2015. Magnetostratigraphy of Chinese loess–paleosol sequences. Earth Sci. Rev. 150, 139–167. https://doi.org/10.1016/j.earscirev.2015.07.009.

Maher, B.A., 2016. Palaeoclimatic records of the loess/palaeosol sequences of the Chinese Loess Plateau. Quat. Sci. Rev. 154, 23–84. https://doi.org/10.1016/j.quascirev.2016.08.004.

Nie, J.S., Stevens, T., Song, Y.G., King, J.W., Zhang, R., Ji, S.C., Gong, L.S., Cares, D., 2014. Pacific freshening drives Pliocene cooling and Asian monsoon intensification. Sci. Rep. 4, 5474 doi: 5410.1038/srep05474.

Pan, B.T., Su, H., Hua, Z.B., Hu, X.F., Gao, H.S., Li, J.J., Kirby, E., 2009. Evaluating the role of climate and tectonics during non-steady incision of the Yellow River: evidence from a 1.24 Ma terrace record near Lanzhou. Quat. Sci. Rev. 28, 3281–3290.

Qiang, X., An, Z., Song, Y., Chang, H., Sun, Y., Liu, W., Ao, H., Dong, J., Fu, C., Wu, F., 2011. New eolian red clay sequence on the western Chinese Loess Plateau linked to onset of Asian desertifi cation about 25 Ma ago. Sci. China Earth Sci. 54, 136–144. https://doi.org/10.1007/s11430-010-4126-5.

Qiu, Z.X., Deng, T., Wang, B.Y., 2004. Early Pleistocene mammalian fauna from longdan. Dongxiang, Gansu, China. Science Press, Beijing, pp. 1–156 (in Chinese with English abstract).

Rolph, T.C., Shaw, J., Derbyshire, E., Wang, J.T., 1989. A detailed geomagnetic record from Chinese loess. Phys. Earth Planet. In. 56, 151–164. https://doi.org/10.1016/0031-9201(89)90044-7.

Song, Y.G., Fang, X.M., Chen, X.L., Torii, M., Ishikawa, N., Zhang, M.S., Yang, S.L., Chang, H., 2017. Rock magnetic record of late Neogene red clay sediments from the Chinese Loess Plateau and its implications for East Asian monsoon evolution. Palaeogeogr. Palaeoclimatol. Palaeoecol. https://doi:10.1016/j.palaeo.2017.09.025 (in press).

Song, Y.G., Wang, Q., An, Z., Qiang, X., Dong, J., Chang, H., Zhang, M., Guo, X., 2017b. Mid-Miocene Climatic Optimum: clay mineral evidence from the red clay succession, Longzhong Basin, Northern China. Palaeogeogr. Palaeoclimatol. Palaeoecol. https://doi.org/10.1016/j.palaeo.2017.1010.1001 (in press).

Sun, D.H., Liu, T.S., Cheng, M.Y., An, Z.S., Shaw, J., 1997. Magnetostratigraphy and palaeoclimate of red clay sequences from Chinese Loess Plateau. Sci. China Earth Sci. 40, 337–343. https://doi.org/10.1007/BF02877564.

Sun, D., Shaw, J., An, Z., Cheng, M., Yue, L., 1998a. Magnetostratigraphy and paleoclimatic interpretation of a continuous 7.2 Ma late Cenozoic eolian sediments from the Chinese Loess Plateau. Geophys. Res. Lett. 25, 85–88. https://doi.org/10.1029/97GL03353.

Sun, D.H., An, Z.S., Shaw, J., Bloemendal, J., Sun, Y.B., 1998b. Magnetostratigraphy and palaeoclimatic significance of late tertiary aeolian sequences in the Chinese Loess Plateau. Geophys. J. Int. 134, 207–212. https://doi.org/10.1046/j.1365-246x.1998.00553.x.

Sun, Y., Clemens, S.C., An, Z., Yu, Z., 2006. Astronomical timescale and palaeoclimatic implication of stacked 3.6-Myr monsoon records from the Chinese Loess Plateau. Quat. Sci. Rev. 25, 33–48. https://doi.org/10.1016/j.quascirev.2005.07.005.

Wang, X.S., Yang, Z.Y., Chen, Y., Hu, J.Y., Tang, L., Mei, S., Løvlie, R., 2015. Deciphering magnetoclimatological patterns of late Early to early Middle Pleistocene loess–paleosol sequences in the western Chinese Loess Plateau. Global Planet. Change 130, 37–46. https://doi.org/10.1016/j.gloplacha.2015.04.003.

Yang, S.L., Ding, Z.L., 2010. Drastic climatic shift at ~2.8 Ma as recorded in eolian deposits of China and its implications for redefining the Pliocene-Pleistocene boundary. Quat. Int. 219, 37–44. https://doi.org/10.1016/j.quaint.2009.10.029.

Zan, J.B., Fang, X.M., Zhang, W.L., Yan, M.D., Zhang, T., 2016. Palaeoenvironmental and chronological constraints on the Early Pleistocene mammal fauna from loess deposits in the Linxia Basin, NE Tibetan Plateau. Quat. Sci. Rev. 148, 234–242. https://doi.org/10.1016/j.quascirev.2016.07.026.

Zan, J.B., Fang, X.M., Yan, M.D., Li, B.S., 2017. New insights into the palaeoclimatic interpretation of the temperature dependence of the magnetic susceptibility and magnetization of Mid-Late Pleistocene loess/palaeosols in Central Asia and the Chinese Loess Plateau. Geophys. J. Int. 208, 663–673. https://doi.org/10.1093/gji/ggw419.

Zhang, J., Li, J.J., Guo, B.H., Ma, Z.H., Li, X.M., Ye, X.Y., Yu, H., Liu, J., Yang, C., Zhang, S.D., Song, C.H., Hui, Z.C., Peng, T.J., 2016. Magnetostratigraphic age and monsoonal evolution recorded by the thickest Quaternary loess deposit of the Lanzhou region, western Chinese Loess Plateau. Quat. Sci. Rev. 139, 17–29. https://doi.org/10.1016/j.quascirev.2016.02.025.